A Dynamic Model of the Phosphate Response System with Synthetic Promoters in Escherichia coli

Cansu Uluşeker[1,4], Jesus Torres[2], José L. García[2], Martin M. Hanczyc[1], Juan Nogales[2], Ozan Kahramanoğulları[3,4]

[1]Centre for Integrative Biology, University of Trento, Trento, Italy
[2]Biological Research Center, Madrid, Spain
[3]Department of Mathematics, University of Trento, Trento, Italy
[4]The Microsoft Research – University of Trento Centre for Computational and Systems Biology, Rovereto, Italy
ozan.kahramanogullari@unitn.it

Abstract

The bacteria *E. coli* have developed one of the most efficient regulatory response to phosphate starvation that is known in detail. Achieving a mechanistic understanding of this system, realized by Pho regulon at the genetic level, has implications for applications in artificial life and for others in biotechnology that exploit such mechanisms. To this end, we present a dynamical model of Pho regulon, coupled with a layered description of its regulation in the experimental conditions of phosphate starvation. The model describes the dynamics of two-component regulatory system together with the key regulatory promoter PhoB and experimental data on promoter PhoA. The model is parameterized according to the feasible range given in the literature, and fitted to the dynamic response of our experimental data on alkaline phosphatase production, coded as Gfp. Sensitivity analysis demonstrates that the rate of Pho transcription has a significant influence over the expression of Pho-controlled genes. Variations in the transcription rates alter the sensitivity of the phosphate starvation response to external phosphate concentration, whereas variations in the translation rates affect the gain of the system. Our model provides a dynamic description of the core determinants of Pho regulon and promoter activities and their response to the change of external phosphate level. As the model architecture is intrinsically open to integrate supplementary layers, together with experimental findings, it should provide insights in investigations on engineering new dynamic sensors and regulators for living technologies.

Introduction

Water pollution is one of the global problems with great impact. Industrial and daily life waste contain inorganic and organic matters, such as heavy metals, which cause the contamination of groundwater (Liandong, 2014). In this respect, the development of eco-friendly bioreactors that input waste water, carbon dioxide, and sunlight to output clean water, electricity, biomass and other mineral resources is a frontier in biotechnology with important implications. We are exploring how the coupling of modeling at different scales with modular architectural design can lead to the production and use of such bioreactors in living technology and synthetic biology applications.

The aim of this project in the context of the European project Living Architecture (LIAR) is to provide an integrated modeling framework across different scales to use metabolites and biochemical transformations to feedback to larger scale outputs of the entire system. To this aim we construct detailed polyphosphate regulation and transcriptional regulatory network models to enable *Escherichia coli* to sense pollutants and relocate towards them. For this purpose, we refine and extend our models with varying levels of detail, e.g., to incorporate equations for ATP efficiency and polyphosphate synthesis and storage, or other aspects of the regulatory mechanism that are relevant for potential applications. For example, for applications in bioremediation and biotechnology industries, it is desirable to control the amount of polyphosphate that can be stored by the cell. The mechanisms controlling such processes as biological phosphorus removal by polyphosphate indicate that metabolic engineering can be used to elucidate some of these mechanisms. A broader understanding of the mechanisms controlling such processes resulting from our framework should lead to improvements in wastewater treatment.

Phosphorous, which is one of the major causes of water quality problems, occurs in wastewater almost solely in the form of phosphates such as inorganic phosphate (Pi) (Liandong, 2014). Microorganisms, which are key players in bioremediation, have potential to treat large amounts of the pollutants and hold promise for renewable sources (Mosa et al., 2016). In particular, the bacteria *E. coli* can take inorganic phosphate and store excess inorganic phosphate in the form of polyphosphates (Wanner, 1996).

In *E. coli*, there are two major phosphate transport systems. One is the low affinity phosphate inorganic transport (Pit) system, and the other is the phosphate specific transport (Pst) system (Wanner et al., 1995). Pit depends on the proton motive force. In other words, it is a coupled transporter of two different ions through the membrane (Wanner, 1996; Harris et al., 2001). Pst system, on the other hand, is Pi-repressible and is induced when the external Pi concentration is depleted (Jansson, 1988).

It is known that Pst system is part of the Pho regulon, which is a global regulatory circuit involved in bacterial phosphate management (Wanner, 1996; Lamarche et al.,

2008). Pst system is controlled by a two-component regulatory system (TCRS), which comprises a histidine kinase (HK) sensor protein and a transciptional response regulator (RR). Pst system's members are induced by pst operon, comprised by Pho regulon (Wanner, 1996; Lamarche et al., 2008; Gardner et al., 2014). The *E. coli* Pho regulon comprises more than 30 genes. Moreover, the expression of these genes has been shown to require the transcription factor PhoB, which upon phosphorylation activates the binding to a consensus promoter region (Wanner, 1996). The final step in this pathway is the induction of many genes including PhoB, PhoR and alkaline phosphatase.

The Pho regulon has been well studied in *E. coli*. All experimental evidence strongly indicates that Pho regulon is controlled by external phosphate limitation rather than internal (Van Dien and Keasling, 1997). When the surrounding environment has abundant phosphate, *E. coli* uses as few resources as possible to facilitate phosphate intake. However, when inorganic phosphate (Pi) becomes low outside the cell, it turns into a growth limiting factor and the cell spends energy to up-regulate the expression of target genes that are used to acquire phosphate. Previous studies have shown that the two-component system, the sensor kinase PhoR and the response regulator PhoB, participate in sensing the Pi level in the environment and regulate the expression of genes that are directly involved in phosphorus assimilation, forming a Pho regulon (Wanner, 1996; Lamarche et al., 2008). Although much is known about the molecular aspects of this signal transduction pathway, a comprehensive and structured mechanistic model of the Pho regulon is currently not available (Van Dien and Keasling, 1997). A better understanding of the Pho regulon controlling such processes resulting from our framework should thus lead to improvements in wastewater treatment.

In our initial model, presented here, we detail a mathematical model for simulating the phosphate starvation response at the genetic level. In a subsequent model, we will extend and refine the purposeful detail of the model to capture temporal and spatial dynamics of the system such as oscillatory behavior that can be supported and propagated by a matrix of interconnected bioreactors. This will allow us to ask whether the system as a whole may function more robustly and operate as an artificial biological organ capable of programmed responsiveness towards the desired outcomes.

In the following, we describe our model, where the behavior of Pho regulon system is expressed within a chemical reaction network representation, and implemented as systems of ordinary differential equations via mass action kinetics. The model includes TCRS members and activation of the Pho regulon by the promoters pPhoB and pPhoA. Experimental data is used to fit the parameters to the feasible physiological range given in the literature, and to determine the relative sensitivity of the simulation to each of these parameters. The simulations with our model provide a seamless dynamic description of the mechanisms. Moreover, sensitivity analysis on parameters demonstrate the influence on the expression of Pho-controlled genes and the gain of the system under variations in transcription efficiency in response to external phosphate concentration.

Material and Methods

Mechanistically, Pi signaling is a negative process. Excessive Pi is required for turning the system off. Activation is the default state and occurs in conditions of Pi limitation (Wanner, 1996; Wanner et al., 1995; Gardner et al., 2014).

Signal transduction by environmental Pi requires seven proteins, which are thought to interact in a membrane associated signaling complex. These Pi signaling proteins include (Wanner, 1996; Wanner et al., 1995)

1. two that are members of the large family of two component systems (TCSs), a sensor histidine kinase PhoR and a response regulator PhoB;

2. four components of the ABC transporter Pst (PstSCAB) an extracellular binding protein (PstS), two transmembrane proteins (PstC, PstA) that form the transmembrane domain (TMD), and a dimer of cytosolic peripheral proteins (PstB), i.e., the nucleotide-binding domain (NBD);

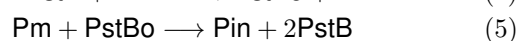3. the chaperone-like PhoR/PhoB inhibitory protein PhoU.

In Fig. 1, the system mechanism is shown. In the starvation condition, when phosphate (Pi) is limited in quantity outside the cell, PstS protein binds to the external phosphate (Pext) following its diffusion to the cell surface (Ps) (Wanner, 1996; Wanner et al., 1995; Lamarche et al., 2008).

$$\text{Pext} \longleftrightarrow \text{Ps} \qquad (1)$$
$$\text{Pst} + \text{Ps} \longleftrightarrow \text{Pst\_Ps} \qquad (2)$$
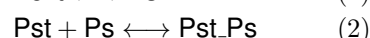
The transmembrane domain of the ABC transporter, that is, PstC and PstA are integral membrane proteins that span the entirety of the membrane. They regulate the translocation of Pi from PstS to the inner membrane, becoming Pm.

$$\text{Pst\_Ps} + \text{PstCA} \longrightarrow \text{PstCA} + \text{Pst} + \text{Pm} \qquad (3)$$

Pi intake happens with the conformational changes in the PstB as a result of ATP binding, also known as ATP-switch model. Principal conformations of the PstB are as follows: (i.) the formation of a closed dimer upon binding two ATP molecules; (ii.) dissociation to an open dimer facilitated (PstBo) by ATP hydrolysis. The switching between the open and closed dimer conformations induces conformational changes in the TMD resulting in substrate translocation of Pi transport from inner membrane (Pm) to the cytosol. This causes an increase in the amount of phosphate in the cell (Pin) (Wanner, 1996; Wanner et al., 1995).

$$2\text{PstB} + 2\text{ATP} \longrightarrow \text{PstBo} + 2\text{ADP} \qquad (4)$$
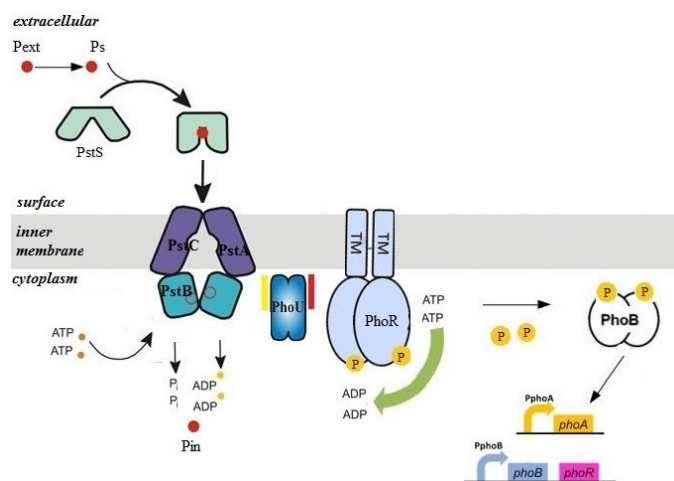$$\text{Pm} + \text{PstBo} \longrightarrow \text{Pin} + 2\text{PstB} \qquad (5)$$
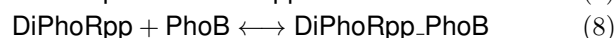
Figure 1: Control of the Pho regulon and transmembrane signal transduction when environmental inorganic phosphate (Pi) is depleted. External Pi binds to the PstS component of the ABC transporter. It is then translocated to the inner membrane domain of the transporter through PstCA. Following this, with the ATP consuming conformational changes of the PstS, Pi is internalized an released to the cytosol. According to current biological model in the literature, PhoR assesses Pi availability by monitoring the activity of Pst transporter. This is done by relaying a signal from PstB via PhoU to PhoR. When the Pi influx is reduced, PhoU does not stabilize PhoR. As a result of this, PhoR becomes free to perform its auto-kinase-phosphotransferase activity, whereby it phosphorylates PhoB. Phosphorylated PhoB then acts in dimers as transcription factor for the operon.

In many eukaryotic receptor families, receptor signaling occurs through signal-mediated dimerization of kinase domains (Gao and Stock, 2009). However, in *E. coli* the perception of stimuli causes alterations in protein-protein interactions within the preformed PhoR dimer. That is, the membrane localized sensor-kinase PhoR is in dimer structure and the signal is relayed to the kinase core domains (Gao and Stock, 2009). PhoR is essential for the control of the PhoB activity as a transcription factor.

Although the exact mechanism is unknown, the current evidence suggests that PhoR and eventually PhoB assess Pi availability by monitoring the activity of Pst transporter via PhoU. That is, PhoU responds to mechanical forces in its interaction with the PstSCAB transporter and transmits that information to PhoR through the PAS domain. This way the signal is relayed from PstB to PhoB (Lamarche et al., 2008). When there is sufficient Pi flux, PhoU stabilizes PhoR (Gardner et al., 2014). The resulting stable conformation of PhoR prevents PhoR from auto-phosphorylation.

Experimental evidence indicates that when PhoU is deleted, PstB not only continues to spend ATP, and trans-

ports Pi, but PhoR is a constitutive PhoB kinase leading to high expression of the Pho regulon genes (Wanner, 1996; Wanner et al., 1995). In mechanistic terms, the low activity of the ABC transporter PstSCAB causes autophosphorylation of the sensor kinase PhoR, which relays the signal to the transcription factor PhoB. That is, when the Pi flux is reduced, PhoU is deactivated. Consequently, the stable interaction between PhoU and PhoR does not take place. PhoR is an auto-kinase and phosphotransferase; PhoR is thus capable of binding ATP, autophosphorylate itself and become active (DiPhoRpp) (Wanner, 1996; Wanner et al., 1995). The inactivation of PhoU allows PhoR to autophosphorylate in dimers, and transfer its phosphoryl group to PhoB resulting in PhoB activation as a DNA binding response regulator, and regulate the operon as an active transcription factor. PhoB has been reported to exist primarily as monomers and phosphorylation greatly enhances dimerization (Jansson, 1988).

$$DiPhoR \longleftrightarrow DiPhoRp \tag{6}$$
$$DiPhoRp \longleftrightarrow DiPhoRpp \tag{7}$$
$$DiPhoRpp + PhoB \longleftrightarrow DiPhoRpp\_PhoB \tag{8}$$
$$DiPhoRpp\_PhoB \longrightarrow DiPhoRp + PhoBp \tag{9}$$
$$DiPhoRp + PhoB \longleftrightarrow DiPhoRp\_PhoB \tag{10}$$
$$DiPhoRp\_PhoB \longrightarrow DiPhoR + PhoBp \tag{11}$$
$$PhoBp + PhoBp \longleftrightarrow DiPhoBpp \tag{12}$$

In E. coli, the sensor histidine kinase PhoR is a bifunctional (paradoxical) enzyme. It catalyzes the phosphorylation of response regulator PhoB and also the dephosphorylation of PhoBp (Shinar et al., 2007; Gao and Stock, 2012).
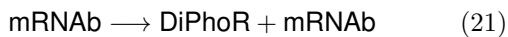
$$DiPhoR + PhoBp \longleftrightarrow DiPhoR\_PhoBp \tag{13}$$
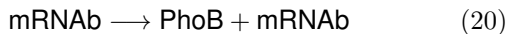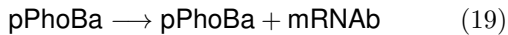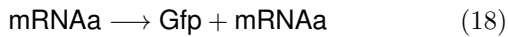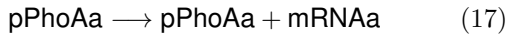$$DiPhoR\_PhoBp \longrightarrow DiPhoR + PhoB \tag{14}$$

Phosphorylated dimer structure PhoB (DiPhoBpp) is enabled for activating Pho regulon by binding to a consensus promoter region. Here, we focus on PhoA and PhoB promoters based on experimental data on PhoA promoter regulation. PhoB and PhoR play important roles in Pho regulon and the phoBR operon is autogenously regulated (Wanner, 1996; Wanner et al., 1995). Thus, the synthesis of the regulatory proteins PhoB and PhoR is under Pho regulon control (Wanner, 1996; Wanner et al., 1995; Warner and Chang, 1987). PhoR expression during phosphate limitation is dependent on the upstream phoB promoter. In fact, the operon structure indicates that phoR gene function requires expression from the phoB promoter (Warner and Chang, 1987).

$$DiPhoBpp + pPhoA \longleftrightarrow pPhoAa \tag{15}$$
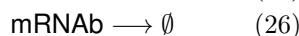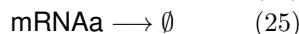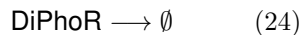$$DiPhoBpp + pPhoB \longleftrightarrow pPhoBa \tag{16}$$
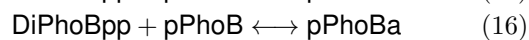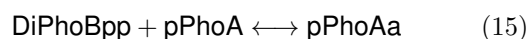
Active promoters pPhoAa and pPhoBa lead to the transcription of mRNA, which carries the information for the

subsequent translation, resulting in protein synthesis.

$$\text{pPhoAa} \longrightarrow \text{pPhoAa} + \text{mRNAa} \qquad (17)$$
$$\text{mRNAa} \longrightarrow \text{Gfp} + \text{mRNAa} \qquad (18)$$
$$\text{pPhoBa} \longrightarrow \text{pPhoBa} + \text{mRNAb} \qquad (19)$$
$$\text{mRNAb} \longrightarrow \text{PhoB} + \text{mRNAb} \qquad (20)$$
$$\text{mRNAb} \longrightarrow \text{DiPhoR} + \text{mRNAb} \qquad (21)$$

With the inclusion of the degradation/dilution terms, we obtain the following reactions.

$$\text{Gfp} \longrightarrow \emptyset \qquad (22)$$
$$\text{PhoB} \longrightarrow \emptyset \qquad (23)$$
$$\text{DiPhoR} \longrightarrow \emptyset \qquad (24)$$
$$\text{mRNAa} \longrightarrow \emptyset \qquad (25)$$
$$\text{mRNAb} \longrightarrow \emptyset \qquad (26)$$

In the following, we investigate the causal relationship between external phosphate-starvation level, the Pho regulon signaling cascade, and the promoter activity. The model is composed of a set of ordinary differential equations (ODE), which are derived from the chemical reaction network above by using the standard translation based on stochiometries and reaction rates. To build the simulation model, we have selected the part of the network from the TCRS, given with PhoB and PhoR, to gene regulation, which is active in starvation conditions. The set of ODEs derived from the chemical reaction network above is listed in Figure 2.

We have ran simulations with the model with an initial state representing the phosphate starvation case. The initial values of the model variables have been derived from the literature or obtained from experimental data. The simulations have been performed for an initial culture containing 0 μM Pext. Prior to Pi starvation, the concentrations of proteins PhoR and PhoB are approximately 0.22 μM. The concentrations of active PhoR and active PhoB are $4 \cdot 10^{-8}$ μM and $6 \cdot 10^{-8}$ μM, as determined by Keasling et al. (Van Dien and Keasling, 1997). With a single plasmid, average mRNA number is 2-3 in *E. coli* (OpenWetWare, 2007). Therefore, the initial states of mRNAa and mRNAb are set to 0.0016 μM, and the initial promoters numbers are set to 10 for each.

The rates of chemical reactions are obtained in accordance with the variability of physiological ranges given in the literature (OpenWetWare, 2007; Alon, 2007; Bloch and Schlesinger, 1973). The extended model includes 26 reactions. The models have been used to reproduce the data and the unknown parameters. We carried out a deterministic parameter estimation procedure, based on using a multi-start approach together with a least squares method. Parameter values taken from literature and the given ranges for the rates are listed in Table 1. The rate values have been selected with respect to the best fit to the physiological range, listed in Table 1, and the dynamics in accordance with the experimental findings in order to avoid discontinuities or states with unrealistic variable values.

$$dGfp(t)/dt = r_{18}.mRNAa(t) - r_{22}.Gfp(t)$$

$$\begin{aligned} dDiPhoR(t)/dt = &\ r_{6r}.DiPhoRp(t) - r_6.DiphoR(t) \\ &+ r_{11}.DiPhoRp\_PhoB(t) + r_{21}.mRNAb(t) \\ &- r_{24}.DiPhoR(t) - r_{13}.DiPhoR(t).PhoBp(t) \\ &+ r_{13r}.DiPhoR\_PhoBp(t) + r_{14}.DiPhoR\_PhoBp(t) \end{aligned}$$

$$\begin{aligned} dDiPhoRp(t)/dt = &\ r_6.DiPhoR(t) - r_{6r}.DiPhoRp(t) \\ &- r_7.DiPhoRp(t) + r_{7r}.DiPhoRpp(t) \\ &+ r_9.DiPhoRpp\_PhoB(t) + r_{10r}.DiPhoRp\_PhoB(t) \\ &- r_{10}.DiPhoRp(t).PhoB(t) \end{aligned}$$

$$\begin{aligned} dDiPhoRp\_PhoB(t)/dt = &\ r_{10}.DiPhoRp(t).PhoB(t) \\ &- r_{10r}.DiPhoRp\_PhoB(t) - r_{11}.DiPhoRp\_PhoB(t) \end{aligned}$$

$$\begin{aligned} dDiPhoRpp(t)/dt = &\ r_7.DiPhoRp(t) - r_{7r}.DiPhoRpp(t) \\ &- r_8.DiPhoRpp(t).PhoB(t) + r_{8r}.DiPhoRpp\_PhoB(t) \end{aligned}$$

$$\begin{aligned} dDiPhoRpp\_PhoB(t)/dt = &\ r_8.DiPhoRpp(t).PhoB(t) \\ &- r_{8r}.DiPhoRpp\_PhoB(t) - r_9.DiPhoRpp\_PhoB(t) \end{aligned}$$

$$\begin{aligned} dPhoB(t)/dt = &\ -r_8.DiPhoRpp(t).PhoB(t) \\ &+ r_{8r}.DiPhoRpp\_PhoB(t) - r_{10}.DiPhoRp(t).PhoB(t) \\ &+ r_{10r}.DiPhoRp\_PhoB(t) + r_{20}.mRNAb(t) \\ &- r_{23}.PhoB(t) + r_{14}.DiPhoR\_PhoBp(t) \end{aligned}$$

$$\begin{aligned} dPhoBp(t)/dt = &\ r_9.DiPhoRpp\_PhoB(t) - 2.r_{12}.PhoBp(t)^2 \\ &+ r_{11}.DiPhoRp\_PhoB(t) + 2.r_{12r}.DiPhoBpp(t) \\ &+ r_{13r}.DiPhoR\_PhoBp(t) - r_{13}.DiPhoR(t).PhoBp(t) \end{aligned}$$

$$\begin{aligned} dDiPhoR\_PhoBp(t)/dt = &\ r_{13}.DiPhoR(t).PhoBp(t) \\ &- r_{13r}.DiPhoR\_PhoBp(t) - r_{14}.DiPhoR\_PhoBp(t) \end{aligned}$$

$$\begin{aligned} dDiPhoBpp(t)/dt = &\ r_{12}.PhoBp(t)^2 - r_{12r}.DiPhoBpp(t) \\ &- r_{15}.DiPhoBpp(t).pPhoA(t) + r_{16r}.pPhoBa(t) \\ &+ r_{15r}.pPhoAa(t) - r_{16}.DiPhoBpp(t).pPhoB(t) \end{aligned}$$

$$\begin{aligned} dpPhoA(t)/dt = &\ -r_{15}.DiPhoBpp(t).pPhoA(t) + r_{15r}.pPhoAa(t) \end{aligned}$$

$$\begin{aligned} dpPhoAa(t)/dt = &\ r_{15}.DiPhoBpp(t).pPhoA(t) - r_{15r}.pPhoAa(t) \end{aligned}$$

$$\begin{aligned} dpPhoB(t)/dt = &\ -r_{16}.DiPhoBpp(t).pPhoB(t) + r_{16r}.pPhoBa(t) \end{aligned}$$

$$\begin{aligned} dpPhoBa(t)/dt = &\ r_{16}.DiPhoBpp(t).pPhoB(t) - r_{16r}.pPhoBa(t) \end{aligned}$$

$$dmRNAa(t)dt = r_{17}.pPhoAa(t) - r_{25}.mRNAa(t)$$

$$dmRNAb(t)/dt = r_{19}.pPhoBa(t) - r_{26}.mRNAb(t)$$

Figure 2: The ODEs for the model reactions.

The unbinding rate of an active transcription factor can vary over many orders of magnitude, depending on its concentration and affinity to the promoter (Alon, 2007). In our model, by assuming that active transcription factors are saturating, we have considered only the forward reactions 15 and 16 for this, and assumed that reverse reactions are negligible within the considered time interval.

Reaction N.	Rate	Fit Value	Literature Value
6	r_6	25.3658	10-100 1/s
6 reverse	r_{6r}	8.1165	$\ll$ 10 1/s
7	r_7	25.3658	10-100 1/s
7 reverse	r_{7r}	8.1165	$\ll$ 10 1/s
8	r_8	100	100 1/μMs
8 reverse	r_{8r}	74.9411	NA
9	r_9	21.3718	17-23 1/s
10	r_{10}	100	100 1/μMs
10 reverse	r_{10r}	74.9411	NA
11	r_{11}	21.3718	17-23 1/s
12	r_{12}	100	100 1/μMs
12 reverse	r_{12r}	74.9411	NA
13	r_{13}	100	100 1/μMs
13 reverse	r_{13r}	74.9411	NA
14	r_{14}	12.95	< 17 1/s
15	r_{15}	10000	10000 1/μMs
16	r_{16}	10000	10000 1/μMs
17	r_{17}	0.0510	0.0025-0.2 1/s
18	r_{18}	0.0302	0.0006-0.05 1/s
19	r_{19}	0.0510	0.0025-0.2 1/s
20	r_{20}	0.0302	0.0006-0.05 1/s
21	r_{21}	0.0302	0.0006-0.05 1/s
22	r_{22}	0.0001	0.000096-0.00079 1/s
23	r_{23}	0.0001	0.000096-0.00079 1/s
24	r_{24}	0.0001	0.000096-0.00079 1/s
25	r_{25}	0.0055	0.0055 1/s
26	r_{26}	0.0055	0.0055 1/s

Table 1: Reactions and deterministic rates obtained from the physiological ranges in (OpenWetWare, 2007; Alon, 2007; Bloch and Schlesinger, 1973).

Experimental Procedure

PhoA promoter was PCR amplified from *E. coli* MG1655 genome and transcriptionally fussed to the translational coupler BCD2 (Mutalik et al., 2013) and the fluorescent msfgfp gene. Subsequently the PphoA::BCD2-msfgpf fragment was cloned using the PacI/HindIII restrictions sites in pSEVA234 plasmid (http://seva.cnb.csic.es/), generating the pSEVA237PphoA vector.

The synthetic promoter Pliar00117 was obtained by PCR using a degenerated primer and the promoter pBG42 (Zobel et al., 2015) as template. The Pliar00117 promoter
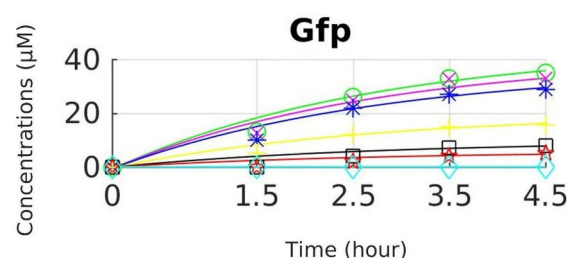

Figure 3: Model fitting and simulation for different concentrations of Pext with respect to experimentally obtained Gfp levels. Each curve represents Gfp dynamics in response to variable Pext concentrations. The experimental data on different Pext conditions are represented as 0 μM Pext with circle $\bigcirc$; 10 μM Pext with cross $\times$; 20 μM Pext with asterisk $*$; 50 μM Pext with plus sign +; 75 μM Pext with square $\square$; 100 μM Pext with star $\star$; 200 μM Pext with diamond $\diamondsuit$. The simulation time course represents the first 4.5 hours.

was transcriptionally fussed to BCD2 and msfgfp gene. The Pliar00117::BCD2-msfgpf fragment was cloned using the PacI/HindIII restrictions sites in pSEVA234 plasmid, generating the pSEVA237Pliar00117 vector. *E. coli* DH10B was used for cloning and for express MsfGFP protein under PphoA or Pliar00117 regulation.

Activity assay of the PphoA and Pliar00117 promoters. *E. coli* DH10B carrying pSEVA237PphoA or pSEVA237Pliar00117 were grown over night at 37°C in MOPS medium (Neidhardt et al., 1974) containing 100 μM KH_2PO_4 to OD600 of 2.0. The bacterial cells were pellet at 1500 xg, room temperature, 10 min and washed twice in MOPS medium without KH_2PO_4. The cells were suspended in 250 μl of MOPS buffer with increases in concentrations of KH_2PO_4 from 0 to 50 mM. The bacterial cell suspensions were loaded in 96-well plates and incubated at 37°C, 200 rpm. The expression of MsfGFP was monitored at different times in a Varioskan Flash spectral scanning multimode reader (Thermo Scientific). αExcitation 488 nm; αEmission 509 nm.

Results

Our main result is the mathematical descriptions of the Pho regulon in phosphate-starvation and the promoter efficiency under the conditions of varying Pext concentrations.

The model has been fitted to the experimental data for different concentration levels of external phosphate that are described by variations in promoter activity rate estimates (Fig. 3). With the optimization fitting model, we have instantiated the promoter activity rates to simulate such variations in external phosphate levels with respect to the data.

The interactions of the TCRS and the operon have been

simulated for 4.5 hours. In Fig. 4, we display the simulation results of the model species dynamics for Pext 0 μM condition. In these simulations, in response to external Pi levels, PhoR dimers are activated, and they are doubly phosphorylated. This results in the activation of the response regulator PhoB, and the consequent dimerization of active PhoB. As a consequence, the promoter activity for PhoA and PhoB rapidly increase. The resulting mRNA production leads to an increase in the concentrations of PhoR and PhoB. The output of the model, in terms of gene regulation, coincided with the input PhoR and PhoB phosphorylation, which resulted in the expected simulation dynamics without the need for external intervention.

Synthetic biology methods provides the means to synthesize constitutive promoters with different activation characteristics. For E. coli, a library of synthetic promoters, which sense Pi with a broad range of sensitivity, have been created. The availability of such a range of promoter activities increases the number of potential regulatory combinations that can be used in the development of Pi-dependent bio-sensors.

We have used the model to explore the effect of the synthetic promoter, where the transcription rate provides a measure of gene expression. The simulation results in Fig. 5 depict the data set with the synthetic promoter Pliar00117 (pPliar00117). As expected, the selected Pliar00117 synthetic promoter has a similar behavior as the pPhoA promoter in starvation conditions; it provides comparable green fluorescent protein expression levels. In other words, synthetic promoter, pPliar00117, is able to express the desired level of Gfp. The simulation results indicate that, within a modular framework, individual promoters can be easy replaced for various tasks.

Fig. 5 depicts the expression profiles at 5 time points with this promoter, whereby the transcription rate of Pho synthetic promoter differs, and the simulations reproduce the experimental data for the promoter. The simulations predict how changes in the genetic components affect the behavior of the circuit. Of all the parameters examined, the rate constant for the promoter activity had the greatest effect on the behavior of the system. Importantly, in starvation conditions, the two component system responds in the same way to the signal with the synthetic promoter or with the PhoA promoter. This suggests that the promoter parameter can be varied to adjust the sensitivity of the Pho regulon to Pext, for example, when all other parameters used for transcription, translation, and degradation of the heterologous protein are the same as those used for the PhoA promoter model.

Sensitivity Analysis

To assess the effect of the estimated rate parameters on the model dynamics, we have performed a parametric sensitivity analysis. For this, we have considered for each reaction the estimated rate in isolation and varied it under mass action law. In the analysis, we have excluded the rate parameters
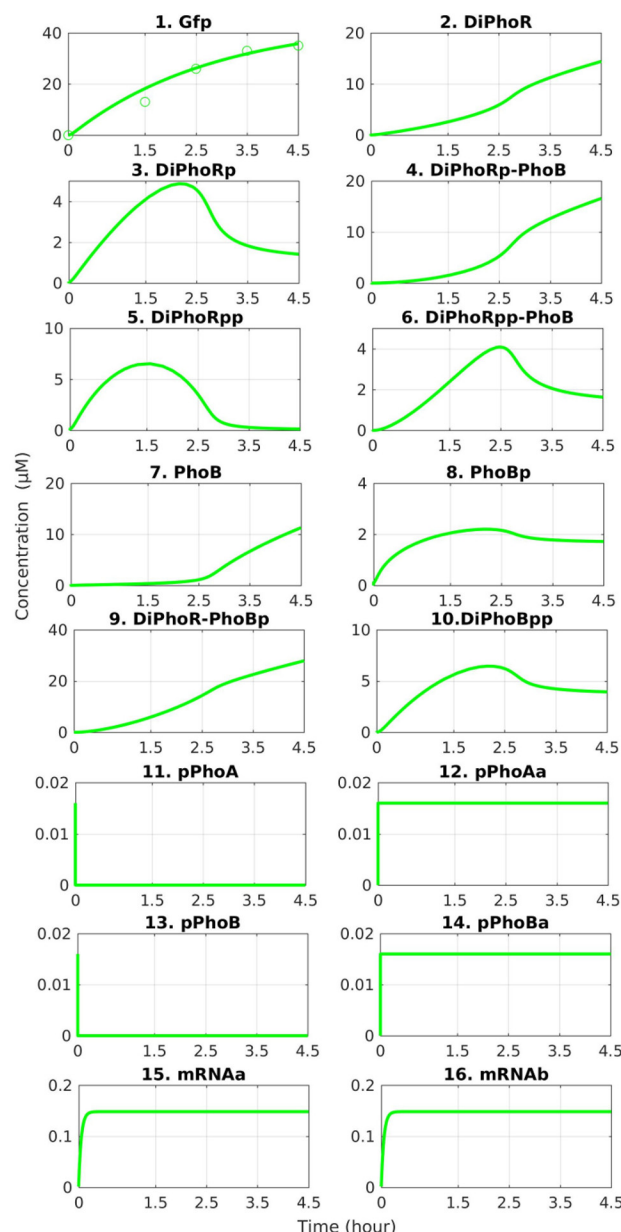

Figure 4: Simulation results with the model for 0 μM Pext. The experimental data is represented with circle $\bigcirc$. The time course for each species until 4.5 hours is depicted.

that have been taken from literature as these parameters have not been estimated. Conversely, the effect of each estimated rate parameter has been analyzed by considering their estimate according to the values in Table 1.

For computing the analysis, each rate parameter estimate has been perturbed by multiplying its value by a factor such that parameters remained within their physiological range. For each value of the parameter, we ran a simulation and measured the impact on the system dynamics on model
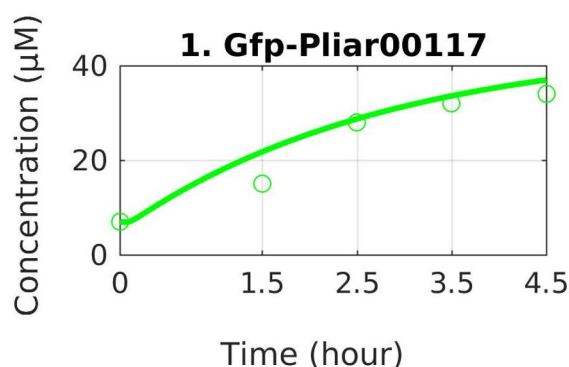
Figure 5: Simulation time course until 4.5 hours for the synthetic promoter Pliar00117 activity and 0 μM Pext. The experimental data is represented with circle $\bigcirc$.
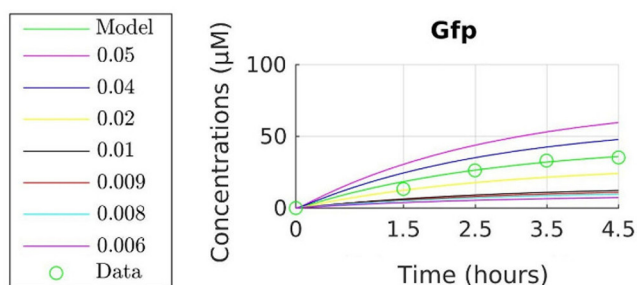

Figure 6: Representative simulation plots of Gfp expression, modeling variations under different conditions. The rate r_{18} of reaction 18 is varied within the physiological range.

species. We ran simulations by varying these fold change values, and we measured the impact of these changes to the system in terms of the area under the curve (AUC) ratio provided by the corresponding simulated behavior in time. AUC ratios computed with the maximum and the minimum considered value of factor and changes are represented with the heatmap in Fig. 7. Below, we consider the most effective reaction rates in further detail.

Translation rates. The translation of mRNA is modeled by the reactions 18, 20 and 21 in the model, and these reactions are governed by the rate constants r_{18}, r_{20} and r_{21} in Table 1. The protein concentrations become proportional to the mRNA levels once the transcription reaches a significant level in the simulations. This becomes the case when sufficient active PhoB (DiPhoBpp) is present in the system to saturate the promoter. The genes encoding PhoR and PhoB are transcribed from the Pho promoter, so a reduction in mRNA resulted in a reduction in DiPhoBpp. This further inhibited alkaline phosphatase production, quantified as Gfp (Fig. 6).

PhoR autophosphorylation. The reactions 6 and 7 with the estimated rates r_6 and r_7 model PhoR phosphorylation. We have applied fold changes within an interval starting from 10 up to 100 that cover possible metabolic perturbations. An increase in these rate constants results in a greater increase in the sensor kinase activity in comparison to the response regulator. Moreover, a greater phosphorylation rate induces a response that is similar to the starvation conditions even with a relatively high external phosphate concentration. These results suggest that the effects of r_6 and r_7 play a significant role in phosphorylation of sensor histidine kinase and the consequent phosphate intake.

Boundaries of disassociation rate. We have provided results that correlate an estimation of the model parameters and their physiological ranges. However, the disassociation rate values depend on the strength of the chemical bonds, which lack ranges. Therefore, we have analyzed these parameters with respect to their impact on the simulation outcome. We have compared the AUC for different values for the rates r_{8r}, r_{12r} and r_{12r} to demonstrate their effect. We have observed that when the values of rates are smaller than 20 1/s, they do not have any visible effect on the system. Moreover, when they are greater than $3.8 \cdot 10^5$ 1/s, they hamper the increase in Gfp.

Discussion

Synthetic life becomes now feasible with the emergence of systems and synthetic biology. While systems biology facilitates the global understanding of natural living systems,

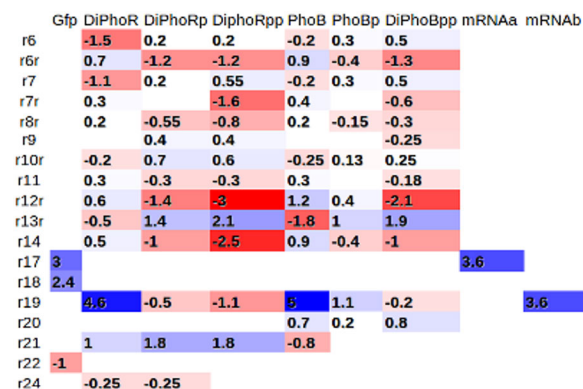|	Gfp	DiPhoR	DiPhoRp	DiphoRpp	PhoB	PhoBp	DiPhoBpp	mRNAa	mRNAb
r6	-1.5	0.2	0.2		-0.2	0.3	0.5		
r6r	0.7	-1.2	-1.2		0.9	-0.4	-1.3		
r7	-1.1	0.2	0.55		-0.2	0.3	0.5		
r7r	0.3		-1.6	0.4			-0.6		
r8r	0.2	-0.55	-0.8		0.2	-0.15	-0.3		
r9		0.4	0.4				-0.25		
r10r	-0.2	0.7	0.6		-0.25	0.13	0.25		
r11	0.3	-0.3	-0.3		0.3		-0.18		
r12r	0.6	-1.4	-3		1.2	0.4	-2.1		
r13r	-0.5	1.4	2.1		-1.8	1	1.9		
r14	0.5	-1	-2.5		0.9	-0.4	-1		
r17	3							3.6	
r18	2.4								
r19	4.6	-0.5	-1.1		6	1.1	-0.2		3.6
r20					0.7	0.2	0.8		
r21	1		1.8	1.8	-0.8				
r22	-1								
r24	-0.25	-0.25							

Figure 7: Heatmap displaying the results of the sensitivity analysis by considering the computed parameter estimates. For each parameter, the maximum and minimum values within its physiological range are considered for simulation, and the area under the curve (AUC) for each species is computed. The difference of the AUC for the maximum and minimum parameter values are then normalized with the AUC of the original model. Red represents the decreasing effect and blue represents the increasing effect.

synthetic biology takes advantage of this better understanding and focuses on the design, construction and optimization of new-to-nature biological functions. Pioneer forward-engineering efforts have addressed the implementation of individual synthetic modules such as logic gates, oscillators, cascades and biosensors (Nielsen et al., 2016; Daniel et al., 2013). However, implementation of complex synthetic biological functions is still challenging as it demands a deep hierarchical control engineering analysis and network integration (He et al., 2016). Analogous to electronic engineering, the implementation of complex synthetic biological functionalities require the integration of sensing, computing and operator modules including signaling, regulatory and metabolic networks. Therefore, new design principles enabling the handling of such complexity, which make model-based approaches mandatory, are needed.

Within this context, a very attractive endeavor for the near future is the possibility of implementing multi-tasks and completely automated synthetic biological devises. For instance the phosphate sensing model constructed here provides an excellent computational framework guiding the construction of a synthetic biological devise for sensing and properly responding to external concentration of phosphate. Further construction of model-based *a la carte* Pi-regulated promoters, when integrated into synthetic regulatory circuits, can be used for driving metabolic modules towards autonomous functions such as Pi-removal and the production of added-value products as a function of the Pi available in domestic gray waters.

Acknowledgements

References

Alon, U. (2007). *An introduction to system biology design principles of biological circuits*. Chapman and Hall/CRC.

Bloch, W. and Schlesinger, M. J. (1973). The phosphate content of escherichia coli alkaline phosphatase and its effect on stopped flow kinetic studies. *JBC*, 248:5794–5805.

Daniel, R., Rubens, J. R., Sarpeshkar, R., and Lu, T. K. (2013). Synthetic analog computation in living cells. *Nature*, 497.

Gao, R. and Stock, A. (2009). Biological insights from structures of two-component proteins. *Annu Rev Microbiol.*, 63.

Gao, R. and Stock, A. (2012). Probing kinase and phosphatase activities of two-component systems in vivo with concentration-dependent phosphorylation profiling. *PNAS*, 110:672–677.

Gardner, S. G., Johns, K. D., Tanner, R., and McCleary, W. (2014). The phou protein from escherichia coli interacts with phor, pstb, and metals to form a phosphate-signaling complex at the membrane. *J Bacteriol*, 196:1741– 1752.

Harris, R. M., Webb, D. C., Howitt, S. M., and Cox, G. B. (2001). Characterization of pita and pitb from escherichia coli. *J Bacteriol.*, 183:5008–5014.

He, F., Murabitom, E., and Westerhoff, H. (2016). Synthetic biology and regulatory networks: where metabolic systems biology meets control engineering. *J R Soc Interface*, 13:1–19.

Jansson, M. (1988). Phosphate uptake and utilization by bacteria and algae. *Kluwer Academic Publishers*, 170:177–189.

Lamarche, M., Wanner, B., Crepin, S., and Harel, J. (2008). The phosphate regulon and bacterial virulence: a regulatory network connecting phosphate homeostasis and pathogenesis. *Federation of European Microbiological Societies*, 32.

Liandong, Z. (2014). *Sustainable biodiesel production from microalgae cultivated with piggery wastewater*. Uni. of Vaasa.

Mosa, K., Saadoun, I., Kumar, K., Helmy, M., and Dhankher, O. (2016). Potential biotechnological strategies for the cleanup of heavy metals and metalloids. *Front Plant Sci.*, 7:303.

Mutalik, V. K., Guimaraes, J. C., Cambray, G., Lam, C., Christoffersen, M. J., Mai, Q. A., Tran, A. B., Paull, M., Keasling, J. D., Arkin, A. P., and Endy, D. (2013). Precise and reliable gene expression via standard transcription and translation initiation elements. *Nature Methods*, 10:354–360.

Neidhardt, F. C., Bloch, P. L., and Smith, D. F. (1974). Culture medium for enterobacteria. *J Bacteriol.*, 119:736–747.

Nielsen, A. A., Der, B. S., Shin, J., Vaidyanathan, P., Paralanov, V., Strychalski, E. A., Ross, D., Densmore, D., and Voigt, C. A. (2016). Genetic circuit design automation. *Science*, 352.

OpenWetWare (2007). Parameter estimation in e.coli. Available at http://www.openwetware.org/wiki/Computational_Biology/Gene_Expression_modeling.

Shinar, G.and Milo, R., Matinez, M., , and Alon, U. (2007). Input output robustness in simple bacterial signaling systems. *Proc. Natl. Acad. Sci.*, 104:19931–19935.

Van Dien, S. J. and Keasling, J. D. (1997). A dynamic model of the escherichia coli phosphate-starvation response. *J. Theor. Biol*, 190:37–49.

Wanner, B. (1996). Phosphorus assimilation and control of the phosphate regulon. In Neidhardt, F., editor, *Escherichia coli and Salmonella typhimurium cellular and molecular biology*, pages 1357–1381. ASM Press, Washington, D.C.

Wanner, B. L., Jiang, W., Kim, S., Yamagata, S., Haldimann, A., and Daniel, L. L. (1995). Are the multiple signal transduction pathways of the pho regulon due to cross talk or cross regulation? In *Regulation of gene expression in Escherichia coli*, pages 297–315. R.G. Landes Company, Texas USA.

Warner, B. and Chang, B. (1987). The phobr operon in escherichia coli k-12. *Bacteriol*, 169:5569–5574.

Zobel, S., Benedetti, I., Eisenbacandh, L., de Lorenzo, V., Wierckx, N., and Blank, L. M. (2015). Tn7-based device for calibrated heterologous gene expression in pseudomonas putida. *ACS Synth Biol.*, 4:1341–1351.